Sector-Resolved Test of Local Position Invariance with Co-Located Cavity–Atom Frequency Ratios

Gary Alcock[1]

[1] *Independent Researcher, Los Angeles, CA, USA*

(Dated: September 3, 2025)

We propose a co-located, two-height comparison of a *solid-state length standard* (evacuated optical cavity) against *atomic frequency standards* to test local position invariance (LPI). In general relativity (GR) all clocks redshift by $\Delta f/f = \Delta\Phi/c^2$; therefore the co-transport ratio $R = f_{\rm cav}/f_{\rm at}$ must be invariant ($\Delta R/R = 0$). We introduce a sector-resolved parameterization in which the cavity and atomic redshifts are

$$\left(\tfrac{\Delta f}{f}\right)^{(M)}_{\rm cav} = \left(\alpha_{\rm w} - \alpha_L^{(M)}\right)\tfrac{\Delta\Phi}{c^2}, \qquad \left(\tfrac{\Delta f}{f}\right)^{(S)}_{\rm at} = \alpha_{\rm at}^{(S)}\tfrac{\Delta\Phi}{c^2},$$

with GR normalization $\boxed{\alpha_{\rm w} = 1,\ \alpha_L^{(M)} = 0,\ \alpha_{\rm at}^{(S)} = 1}$. The measurable ratio slope is

$$\frac{\Delta R^{(M,S)}}{R^{(M,S)}} = \xi^{(M,S)}\frac{\Delta\Phi}{c^2}, \qquad \xi^{(M,S)} = \alpha_{\rm w} - \alpha_L^{(M)} - \alpha_{\rm at}^{(S)}.$$

To remove gauge/identifiability degeneracies, we report the three *physically identifiable* combinations

$$\delta_{\rm tot} \equiv \alpha_{\rm w} - \alpha_L^{\rm ULE} - \alpha_{\rm at}^{\rm Sr}, \quad \delta_L \equiv \alpha_L^{\rm Si} - \alpha_L^{\rm ULE}, \quad \delta_{\rm at} \equiv \alpha_{\rm at}^{\rm Yb} - \alpha_{\rm at}^{\rm Sr},$$

for which the four measured slopes obey

$$\begin{aligned} \xi^{(\rm ULE,Sr)} &= \delta_{\rm tot}, \\ \xi^{(\rm ULE,Yb)} &= \delta_{\rm tot} - \delta_{\rm at}, \\ \xi^{(\rm Si,Sr)} &= \delta_{\rm tot} - \delta_L, \\ \xi^{(\rm Si,Yb)} &= \delta_{\rm tot} - \delta_L - \delta_{\rm at}. \end{aligned}$$

This over-determined 4→3 system is solved by generalized least squares (GLS) with full covariance, separating solid-state length, atomic-structure, and residual wave-propagation responses. We specify metrology-grade geopotential determination (beyond $g\Delta h$), elastic-sag modeling with an orientation-flip control, dual-wavelength dispersion and thermo-optic bounds, and a quantitative noise/systematics budget yielding projected 68/95% confidence intervals on $(\delta_{\rm tot}, \delta_L, \delta_{\rm at})$ for $\Delta h = 30$–$100\,\mathrm{m}$.

I. Motivation and context

The Einstein equivalence principle (EEP) asserts that non-gravitational clocks share the same fractional gravitational redshift [1]. Optical clocks have verified redshift over mm–km scales [2–4]; cavity tests constrain LLI at 10^{-18} [5–7]; matter-wave interferometry probes related aspects [8–11]; composition-dependent tests bound WEP violations [12–14]. Yet a *co-located* redshift comparison between a solid-state length standard and atomic standards across a vertical potential change has not set sector-resolved bounds at $\lesssim 10^{-16}$. Our goal is to provide that sector resolution with a minimal, over-determined design.

II. Identifiable sector parameters and GR limit

We adopt the GR normalization $\alpha_{\rm w} = 1$, $\alpha_L^{(M)} = 0$, $\alpha_{\rm at}^{(S)} = 1$, so the cavity behaves as any clock in GR and $\Delta R/R = 0$. Because adding a common offset to $\{\alpha_{\rm w}, \alpha_L^{\rm ULE}, \alpha_L^{\rm Si}\}$ or to $\{\alpha_{\rm w}, \alpha_{\rm at}^{\rm Sr}, \alpha_{\rm at}^{\rm Yb}\}$ leaves slopes invariant, only three combinations are identifiable. We therefore report $(\delta_{\rm tot}, \delta_L, \delta_{\rm at})$ as defined above. The linear system for $\boldsymbol{\xi} = \{\xi^{(\rm ULE,Sr)}, \xi^{(\rm ULE,Yb)}, \xi^{(\rm Si,Sr)}, \xi^{(\rm Si,Yb)}\}^\top$ and $\boldsymbol{\delta} = \{\delta_{\rm tot}, \delta_L, \delta_{\rm at}\}^\top$ is

$$\boldsymbol{\xi} = \mathbf{B}\,\boldsymbol{\delta}, \quad \mathbf{B} = \begin{pmatrix} 1 & 0 & 0 \\ 1 & 0 & -1 \\ 1 & -1 & 0 \\ 1 & -1 & -1 \end{pmatrix},$$

which is full-rank.

A. GLS estimator and covariance

With slope covariance $\mathbf{C}_\xi$ (from repeated cycles including configuration-dependent nuisance parameters), the GLS solution and parameter covariance are

$$\hat{\boldsymbol{\delta}} = (\mathbf{B}^\top \mathbf{C}_\xi^{-1}\mathbf{B})^{-1}\mathbf{B}^\top \mathbf{C}_\xi^{-1}\boldsymbol{\xi}, \qquad \mathbf{C}_\delta = (\mathbf{B}^\top \mathbf{C}_\xi^{-1}\mathbf{B})^{-1}.$$

We report 68/95% CIs from $\mathbf{C}_\delta$ and test GR ($\boldsymbol{\delta} = \mathbf{0}$) with $\chi^2 = \hat{\boldsymbol{\delta}}^\top \mathbf{C}_\delta^{-1}\hat{\boldsymbol{\delta}}$.

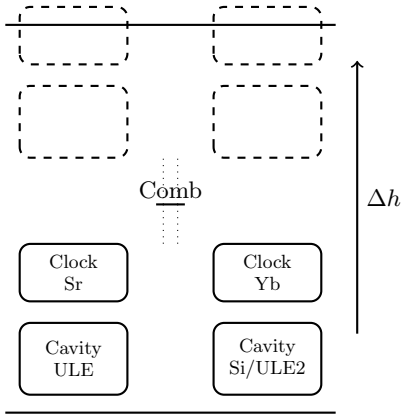

FIG. 1. At each height, PDH-locked cavity lasers (two materials/builds) and co-located Sr and Yb clocks are compared by a comb to form four ratios $R^{(M,S)}$. Two stationary windows (bottom/top) per cycle give four slopes $\xi^{(M,S)}$, which determine $(\delta_{\rm tot}, \delta_L, \delta_{\rm at})$ via GLS with full covariance.

III. Experimental concept and cadence

Two evacuated cavities (ULE at RT; Si cryogenic *or* a second ULE with distinct geometry/coatings) provide $f_{\rm cav}^{(M)}$ via PDH. Co-located Sr and Yb optical clocks provide $f_{\rm at}^{(S)}$. A self-referenced comb measures the four ratios $R^{(M,S)}$ simultaneously. The apparatus measures at two heights $\Delta h = 30$–100 m; *no data are taken during motion*. Each cycle uses two stationary windows (bottom/top). Per-slope estimates are the ratio differences divided by the metrology-grade $\Delta\Phi/c^2$ (Sec. IV).

IV. Geodesy and potential modeling

We determine $\Delta\Phi$ with geodetic methods, not $g\Delta h$ approximations. Heights are tied by differential leveling (or laser trackers) referenced to benchmarks with geoid models; local gravity is measured by relative gravimeters; solid Earth/ocean tides, atmospheric loading, and polar motion corrections are applied for the measurement epochs; the geopotential number difference is converted to $\Delta\Phi$ with uncertainties (few $\times 10^{-18}$ fractional over 30–100 m is routine in chronometric geodesy). The $\Delta\Phi$ uncertainty enters the slope covariance $\mathbf{C}_\xi$ as a multiplicative error common to all four slopes.

V. Cavity mechanics under transport

Vertical relocation changes load paths, tilt, and gravity gradient; supports can induce elastic sag independent of redshift. We bound this with:

- **Elastic model:** Treat spacer as a beam of length L, modulus E, second moment I, effective weight W, with support spacing optimized to null first-order sag. The static deflection $\delta L \sim \kappa W L^3/(EI)$ (geometry-dependent $\kappa \ll 1$); we target $|\delta L|/L < 3 \times 10^{-16}$ per window, verified at both heights.
- **Orientation flip:** Rotate each cavity by 180° (around its optical axis or swap support orientation) at each height. A mechanical-length artifact changes sign; a genuine redshift does not. The flip difference enters $\mathbf{C}_\xi$ for robust profiling.
- **Tilt budget:** Measure platform tilt; require $\leq 100\,\mu$rad with shimming. Beam-walk and mirror bending are modeled; residuals are bounded $< 10^{-16}$.

VI. Dual-wavelength check and dispersion bound

Each cavity is probed at two wavelengths λ_1, λ_2 separated by $\gtrsim 50$ nm within the low-loss band (e.g., 698/1064 nm or 934/1064 nm). Residual mirror-coating dispersion and thermo-refractive effects can bias the inferred slope. A first-order bound gives

$$|\Delta\xi_{\rm disp}| \lesssim \left|\frac{\partial \ln n_{\rm eff}}{\partial \ln \lambda}\right| \cdot \left|\frac{\Delta T}{\Delta\Phi/c^2}\right| + \left|\frac{\partial \ln L}{\partial \ln \lambda}\right| \cdot \left|\frac{\Delta T}{\Delta\Phi/c^2}\right|,$$

using measured $\partial n/\partial T$, coating dispersion, and window ΔT. We require

$$|\xi_{\lambda_1} - \xi_{\lambda_2}| < 0.1\,|\xi|_{\rm targ} \quad \text{and} \quad < 2\sigma_\Delta,$$

so dispersion/thermo-optic bias contributes $\leq 10\%$ of a per-slope target and $\lesssim 2\%$ in the GLS solution (typical cond$(\mathbf{B}) \sim \mathcal{O}(1)$). Polarization is fixed and monitored; birefringence is bounded with a polarization-swap control.

VII. Environmental thresholds and hardware swaps

Stationary windows: locks re-acquired; platform acceleration RMS $< 10^{-3}\,g$ (1–100 Hz); linear drift $< 3 \times 10^{-15}$ per 300 s with $R^2 > 0.98$; pod temperature stability < 10 mK; pressure stability $< 10^{-2}$ mbar; magnetic field drift $< 10\,\mu$T with reversal every other window. **Swaps:** Every K=4 cycles (or ∼1 h), swap mirror sets/mount orientation, interchange Sr/Yb comb feeds, and permute detection electronics. Configuration offsets $\{\delta_c\}$ are profiled; induced correlations are encoded in $\mathbf{C}_\xi$.

VIII. Noise and systematics budget

We model the ratio Allan variance as $\sigma_y^2(\tau) = h_{-1}/\tau + h_0 + h_{+1}\tau$ (white-FM, flicker-FM, random-walk-FM). Table I lists representative per-window contributions for 300 s windows; common-mode terms are handled in $\mathbf{C}_\xi$.

For $\Delta h = 100$ m, $(g\Delta h/c^2) = 1.09 \times 10^{-14}$. A per-slope target sensitivity $|\xi|_{\rm targ} \sim 0.05$ is reachable in tens of minutes under the conservative envelope; GLS then yields projected 68/95% CIs on $(\delta_{\rm tot}, \delta_L, \delta_{\rm at})$. A simulated corner plot (Supplemental) shows expected contours from mock $\boldsymbol{\xi}$ and full $\mathbf{C}_\xi$.

IX. Practical implementation choices

A cryogenic Si cavity is attractive but not essential. A fully room-temperature 2×2 using two ULE builds (different geometry/coatings) suffices to determine

TABLE I. Illustrative per-window fractional uncertainties (300 s). Numbers indicate target control levels used in projections; correlated terms enter $\mathbf{C}_\xi$.

Effect	Cavity/Comb	Clocks (Sr/Yb)
White FM ($h_{-1}^{1/2}$)	$5\times10^{-15}/\sqrt{\tau}$	$2\times10^{-15}/\sqrt{\tau}$
Flicker floor ($h_0^{1/2}$)	3×10^{-16}	2×10^{-16}
Random-walk ($h_{+1}^{1/2}$)	$< 10^{-17}/\sqrt{\text{s}}$	$< 10^{-17}/\sqrt{\text{s}}$
Thermal drift (fit residual)	3×10^{-15}	5×10^{-16}
Comb path asymmetry	5×10^{-16}	—
Magnetic (2nd-order Zeeman)	—	5×10^{-16}
Pressure/refractive (residual)	$< 1\times10^{-16}$	—
Geodesy ($\Delta\Phi$ scale)	$< 3\times10^{-17}$ (common)	

$(\delta_{\rm tot}, \delta_L, \delta_{\rm at})$. If Si is used, a compact cryostat and thermal-settling data should demonstrate the window criteria are achievable.

X. Reporting and interpretation

Primary results are the four slopes with full covariance and the GLS estimates $\hat{\boldsymbol{\delta}}$ with $\mathbf{C}_\delta$, reported as 68/95% CIs. GR corresponds to $\boldsymbol{\delta} = \mathbf{0}$. We recommend reporting in the δ-basis; SME mappings are model-dependent and provided as context only.

XI. Conclusions

The sector-resolved, over-determined cavity–atom comparison isolates solid-state length, atomic-structure, and wave-propagation redshift responses and provides clean, co-located LPI/UCR tests across 30–100 m height differences. The corrected GR limit, identifiable δ-basis, metrology-grade geodesy, elastic-sag controls, and quantitative noise/systematics budget establish this as a rigorous experimental framework; with initial data setting competitive bounds, it would naturally transition to a full GR test.

A. Note on SME context

Isotropic SME combinations affecting photon propagation and matter sectors can be related qualitatively to $(\delta_{\rm tot}, \delta_L, \delta_{\rm at})$. Because mappings depend on material and atomic structure, we report bounds primarily in the δ-basis and defer coefficient extraction to future, system-specific work.

Acknowledgments

We thank colleagues in precision metrology for advice on geodesy, vibration immunity, and fieldable clocks/comb systems.

[1] C. M. Will, "The Confrontation between General Relativity and Experiment," Living Rev. Relativ. **17**, 4 (2014). doi:10.12942/lrr-2014-4

[2] C. W. Chou, D. B. Hume, T. Rosenband, D. J. Wineland, "Optical Clocks and Relativity," Science **329**, 1630–1633 (2010). doi:10.1126/science.1192720

[3] W. F. McGrew *et al.*, "Atomic clock performance enabling geodesy below the centimetre level," Nature **564**, 87–90 (2018). doi:10.1038/s41586-018-0738-2

[4] T. Bothwell *et al.*, "Resolving the gravitational redshift across a millimetre-scale atomic sample," Nature **602**, 420–424 (2022). doi:10.1038/s41586-021-04349-7

[5] C. Eisele, A. Y. Nevsky, S. Schiller, "Laboratory Test of the Isotropy of Light Propagation at the 10^{-17} Level," Phys. Rev. Lett. **103**, 090401 (2009). doi:10.1103/PhysRevLett.103.090401

[6] S. Herrmann *et al.*, "Rotating Optical Resonator Experiment Testing Lorentz Invariance at the 10^{-17} Level," Phys. Rev. D **80**, 105011 (2009). doi:10.1103/PhysRevD.80.105011

[7] M. Nagel *et al.*, "Direct Terrestrial Test of Lorentz Symmetry in Electrodynamics to 10^{-18}," Nat. Commun. **6**, 8174 (2015). doi:10.1038/ncomms9174

[8] A. D. Cronin, J. Schmiedmayer, D. E. Pritchard, "Optics and Interferometry with Atoms and Molecules," Rev. Mod. Phys. **81**, 1051–1129 (2009). doi:10.1103/RevModPhys.81.1051

[9] P. Asenbaum, C. Overstreet, M. Kim, J. Curti, M. A. Kasevich, "Atom-Interferometric Test of the Equivalence Principle at the 10^{-12} Level," Phys. Rev. Lett. **125**, 191101 (2020). doi:10.1103/PhysRevLett.125.191101

[10] A. Roura, "Gravitational Redshift in Quantum-Clock Interferometry," Phys. Rev. X **10**, 021014 (2020). doi:10.1103/PhysRevX.10.021014

[11] P. Wolf, L. Blanchet, C. J. Bordé, S. Reynaud, C. Salomon, C. Cohen-Tannoudji, "Does an Atom Interferometer Test the Gravitational Redshift at the Compton Frequency?" Class. Quantum Grav. **28**, 145017 (2011). doi:10.1088/0264-9381/28/14/145017

[12] S. Schlamminger, K.-Y. Choi, T. A. Wagner, J. H. Gundlach, E. G. Adelberger, "Test of the Equivalence Principle Using a Rotating Torsion Balance," Phys. Rev. Lett. **100**, 041101 (2008). doi:10.1103/PhysRevLett.100.041101

[13] T. A. Wagner, S. Schlamminger, J. H. Gundlach, E. G. Adelberger, "Torsion-balance tests of the weak equivalence principle," Class. Quantum Grav. **29**, 184002 (2012). doi:10.1088/0264-9381/29/18/184002

[14] P. Touboul *et al.*, "MICROSCOPE Mission: First Results of a Space Test of the Equivalence Principle," Phys. Rev. Lett. **119**, 231101 (2017). doi:10.1103/PhysRevLett.119.231101

[15] S. B. Koller *et al.*, "Transportable Optical Lattice Clock with 10^{-16} Uncertainty," Phys. Rev. Lett. **118**, 073601 (2017). doi:10.1103/PhysRevLett.118.073601

[16] J. Grotti *et al.*, "Geodesy and Metrology with a Transportable Optical Clock," Nat. Phys. **14**, 437–441 (2018). doi:10.1038/s41567-017-0042-3

[17] N. Poli, C. W. Oates, P. Gill, G. M. Tino, "Optical atomic clocks," Riv. Nuovo Cimento **36**, 555–624 (2013) [published 2014]. doi:10.1393/ncr/i2013-10095-5

[18] N. Nemitz *et al.*, "Frequency ratio of Yb and Sr clocks with 5×10^{-17} uncertainty at 150 s averaging time," Nat. Photonics **10**, 258–261 (2016). doi:10.1038/nphoton.2016.20

[19] T. Kessler *et al.*, "A sub-40-mHz-linewidth laser based on a silicon single-crystal optical cavity," Nat. Photonics **6**, 687–692 (2012). doi:10.1038/nphoton.2012.217

[20] T. L. Nicholson *et al.*, "Systematic evaluation of an atomic clock at 2×10^{-18} total uncertainty," Nat. Commun. **6**, 6896 (2015). doi:10.1038/ncomms7896

[21] S. Häfner *et al.*, "8 mHz linewidth lasers," Opt. Lett. **40**, 2112–2115 (2015). doi:10.1364/OL.40.002112

[22] D. G. Matei *et al.*, "1.5 μm lasers with sub-10 mHz linewidth," Phys. Rev. Lett. **118**, 263202 (2017). doi:10.1103/PhysRevLett.118.263202

[23] W. Zhang *et al.*, "Ultrastable Silicon Cavity in a Continuously Operating Closed-Cycle Cryostat," Phys. Rev. Lett. **119**, 243601 (2017). doi:10.1103/PhysRevLett.119.243601

[24] V. A. Kostelecký, N. Russell, "Data Tables for Lorentz and CPT Violation," Rev. Mod. Phys. **83**, 11–31 (2011). doi:10.1103/RevModPhys.83.11